Medical Engineering and Physics 70 (2019) 62–71

Contents lists available at ScienceDirect

Medical Engineering and Physics

journal homepage: www.elsevier.com/locate/medengphy

Technical note

Development and validation of a semi-automatic landmark extraction method for mesh morphing

Jun Wu[a,c], Meiling Cai[a], Junyi Li[b,*], Libo Cao[c], Liangliang Xu[d], Na Li[e], Jingwen Hu[f]

[a] College of Engineering and Design, Hunan Normal University, Changsha, Hunan, China
[b] Urban Development Business Unit, CRRC Zhuzhou institute Co., Ltd, Zhuzhou, Hunan, China
[c] State Key Laboratory of Advanced Design and Manufacturing for Vehicle Body, Hunan University, Changsha, Hunan, China
[d] Wuhu Jinmao Liquid Sicence & Technology Co. Ltd, Wuhu, Anhui, China
[e] Xiangya 3rd hospital, Central South University, Changsha, Hunan, China
[f] University of Michigan Transportation Research Institute, Ann Arbor, MI, USA

ARTICLE INFO

Article history:
Received 1 March 2018
Revised 14 April 2019
Accepted 26 April 2019

Keywords:
Radial basis function
Landmarks
FE model
Geometric accuracy

ABSTRACT

Currently, landmark-based mesh morphing technology is widely used to rapidly obtain meshes with specific geometry, which is suitable to develop parametric human finite element (FE) models. However it takes too much time for landmark extraction to obtain high geometric accuracy. The purpose of this study is to develop and validate a semi-automatic landmark extraction method to reduce the time of manual selection of landmarks without sacrificing the accuracy of identifying landmarks in the process of mesh morphing. A few contour edge landmarks were extracted manually. Mathematical landmarks and pseudo-landmarks were extracted automatically by user-defined algorithm. The radial basis function (RBF) was used to morph the baseline FE model into the target geometry based on these landmarks. The cervical vertebra (C5), rib (R7) and femur were selected as the target geometries to verify the effectiveness of the method. The maximum mean geometric error of the three types of target geometries was less than 1 mm. The mesh quality of the morphed FE model was similar to that of the baseline FE model. Compared to the traditional manual method, 2/3 to 3/4 of the time for landmark extraction was saved by the semi-automatic method.

1. Introduction

Mesh morphing is an interpolation technique that adapts template meshes to the target geometry through a seamless transition. Although this technique was introduced in late 1990s [1], the parametric finite element (FE) modeling concept has become popular only in recent years. Table 1 lists some studies on the development of parametric human FE models. In the area of parametric FE modeling, the mesh morphing method is used to adapt the FE model of human body to other geometries smoothly without developing new FE meshes. Despite the difference among mesh morphing methods, these methods can be divided into two types: landmark-based mesh morphing [2–8] and surface-matching-based mesh morphing [9–11]. Because the relationship between human characteristics and landmarks on human geometry can be easily obtained through regression analysis, landmark-based mesh morphing is often used to develop parametric human FE models, which have been used to investigate the effects of human characteristics on injuries, including variations in bone geometry, material properties, age, gender, stature, and body mass index (BMI) [4–8,12,13]. Nevertheless, thousands of corresponding landmarks on target geometries must be extracted manually from Computed Tomography (CT) or Magnetic Resonance Imaging (MRI) scan data in the process of developing parametric human FE models [4,5,8]. In order to quantify the age effects on the head morphology and the impact responses, Li et al. [5] developed a parametric pediatric head FE model based on head CT scans from 56 children aged 0–3 years old. Sixty landmarks on one half of each child's skull and a total of 3360 landmarks were identified manually. Shi et al. [4] developed a statistical rib cage geometry model to describe variations in rib shape, size and cross-sectional area with changes in age, sex, stature and BMI. On the left side of each subject's ribcage, 464 landmarks were identified manually, and a total of 41,296 landmarks were collected from 89 rib cage CT scans. With the purpose of describing variation in femur geometry with age, femur length, and BMI for men and women, Klein et al. [8] manually extracted 59 landmarks on each femur and a total of 5782 landmarks on 98 femur CT scans to develop a statistical femur geometry model.

In previous studies, the identification and extraction of corresponding landmarks on the target geometry and baseline model

* Corresponding author.
E-mail address: beifanging@163.com (J. Li).

https://doi.org/10.1016/j.medengphy.2019.04.007
1350-4533/

Table 1
An overview of recent parametric human FE models.

Body region	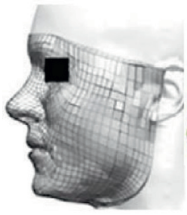	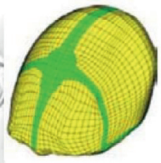	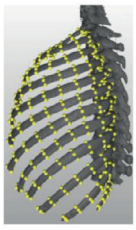		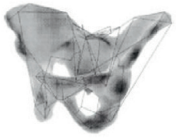
	Face	Head	Rib cage		Pelvis
Morphing method	Mesh-Matching algorithm	Radial basis function	Radial basis function	Radial basis function	Kriging
Morphing type	Surface matching	Landmark based	Landmark based	Landmark based	Landmark based
Reference	Bucki[10]	Li[3]	Shi[4]	Wang[6]	Besnault[2]
Body region					
		Femur`			Whole-body
Morphing method	Surface matching and Laplace smoothing	Radial basis function	Elastic volumetric registration	Radial basis function	Radial basis function
Morphing type	Surface matching	Landmark based	Surface matching	Landmark based	Landmark based
Reference	Bryan[9]	Grassi [14]	Couteau[11]	Klein[8]	Zhang[7]

mainly used the manual method [4,5,8]. Although these manually selected landmarks can meet the requirements of developing FE models, there exist three problems. First, identifying and extracting landmarks manually are highly time-consuming. Previous studies have focused only on a certain part of the human body, namely, the head, rib cage, and femur, as mentioned above. For a whole-body human FE model, the number of landmarks increases significantly, as does the operator workload. Second, it is difficult for operators to extract non-anatomic landmarks, because these landmarks are not easily distinguished. Generally, these landmarks are determined based on the relative positions to the anatomic landmarks [5,8]. Third, for extracting a specific landmark in a target geometry model, different landmark locations may be obtained from different operators, leading to an inconsistent accuracy of the morphed geometry. Even for an operator extracting the same landmark from different target geometries, the accuracy of the landmark can vary.

Therefore, to reduce the time and difficulty in identifying and extracting landmarks and to ensure the geometric accuracy and mesh quality of parametric human FE models developed by the method of radial basis function (RBF) mesh morphing, this study aims to (1) develop a method of semi-automatically extracting landmarks and (2) validate the method by applying it to different bones of the human body.

2. Materials and methods

2.1. Landmarks classification

The landmarks were classified into three subgroups according to their location on the target geometry, as shown in Figure 1.

(1) Contour edge landmarks: In the geometric edge position, these landmarks are easily identified and extracted. These landmarks are used to determine the edge contour of the geometry.
(2) Mathematical landmarks: There landmarks have mathematical or geometric property, i.e., high curvature.
(3) Pseudo-landmarks: These landmarks are not obvious to identify and are evenly distributed between the contour edge landmarks and mathematical landmarks on the geometry.

Note: The landmarks on skeletons are usually divided into anatomic and non-anatomic landmarks. The anatomic landmarks

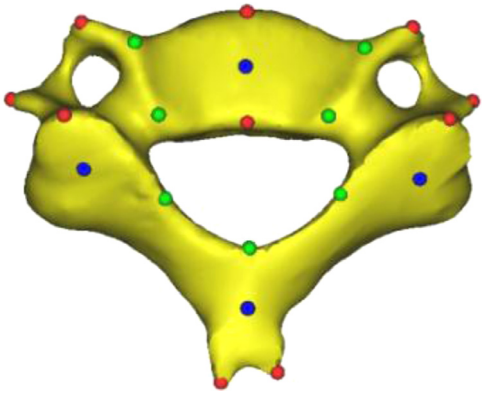

Figure 1. Landmarks are classified into three subgroups based on the position of the landmark on the geometry. Red points represent contour edge landmarks (●). Green points represent mathematical landmarks (●). Blue points represent pseudo-landmarks (●). (For interpretation of the references to color in this figure legend, the reader is referred to the web version of this article.)

were classified into contour edge landmarks and mathematical landmarks, and the non-anatomic landmarks were defined as pseudo-landmarks.

2.2. Procedure for semi-automatically extracting landmarks

A flowchart of landmarks extracted by the semi-automatic method is shown in Figure 2. This method is mainly used to morph a baseline model into the target geometry using mesh morphing techniques based on corresponding landmarks extracted from both the baseline model and the target geometry. Details of the method are indicated as follows:

Specifically, mesh morphing was performed three times to make the baseline model approach the target geometry gradually. Preliminary morphing was conducted with manually selected contour edge landmarks. Secondary morphing was conducted with contour edge landmarks and automatically extracted mathematical landmarks. The final morphing was conducted with contour edge landmarks, mathematical landmarks and automatically extracted pseudo-landmarks, after which the final morphed model with accurate geometry and high mesh quality was obtained.

2.3. Target geometry model and baseline FE model

Considering the diversity of human skeletons, the fifth cervical vertebra (C5), the seventh rib (R7) and the femur, each of two different ages, were selected as the target geometries to study the effectiveness of the method. The six target geometries were numbered from No. 1 to No. 6. All six CT scans were obtained from the volunteer database of the Xiangya Third Hospital of Central South University, China. Ethical approval was obtained by an institutional review board of the Third Xiangya Hospital (Approval number: 2017-S270). The CT scans, which had a resolution of 512 × 512 pixels with a 1.25 mm spacing between slices, were acquired from individuals without apparent trauma or pathology. The display field of view of the CT data was 250 mm, resulting in a resolution of 0.49 mm per pixel. CT image segmentation and 3D reconstruction were performed using Mimics (Materialise, Leuven, Belgium), which included the following operations: first, create a mask for target bones using the bone adaptive threshold; second, isolate the specific bone using “region growing”, third, obtain the 3D model of the target bone using “calculate 3D from mask”. Then the point cloud data for the outer surface of the target geometry model were obtained.

The baseline FE model used in this study was a 10-year-old human body FE model created by Wayne State University, which had detailed anatomical characteristics and was validated at the component level (head, neck [15,16]; thorax [17,18]; thorax/abdomen pelvis [19]; lower extremity [19]) and system level (standing model [20]; sitting model [20]). The C5, R7 and femur FE model with 2D facet elements and 3D solid elements were extracted from the baseline FE model using Hypermesh 11.0 (Altair, U.S.). Information about the six samples and three baseline FE models is listed in Table 2.

2.4. Extraction of landmarks and RBF mesh morphing

2.4.1. Landmarks on the baseline model

The methods of semi-automatically extracting landmarks and RBF mesh morphing were applied to six samples. The C5 target geometry (sample No 1) is taken as an example.

A total of 100 landmarks consisting of 25 contour edge landmarks, 10 mathematical landmarks and 65 pseudo-landmarks were extracted manually on the C5 baseline FE mesh. The landmarks on the target geometry should be corresponding to those on the baseline model.

2.4.2. Manual extraction of contour edge landmarks and preliminary morphing

Twenty five contour edge landmarks corresponding to the C5 FE mesh were extracted manually on C5 target geometry. Then RBF mesh morphing was used to morph the 2D C5 baseline FE mesh into C5 target geometry according to the 25 corresponding contour edge landmarks. Meanwhile, mathematical landmarks and pseudo-landmarks on the 2D C5 FE mesh were morphed into a position close to the target geometry.

2.4.3. Automatic extraction of mathematical landmarks and secondary morphing

Several steps were involved in automatically extracting mathematical landmarks on the C5 target geometry corresponding to those on the FE mesh. As shown in Figure 3a, it is assumed that a mathematical landmark P on the preliminary morphed C5 FE mesh corresponds to landmark Pt on the C5 target geometry. First, the unit normal vector of P was calculated. Then, a point P', whose

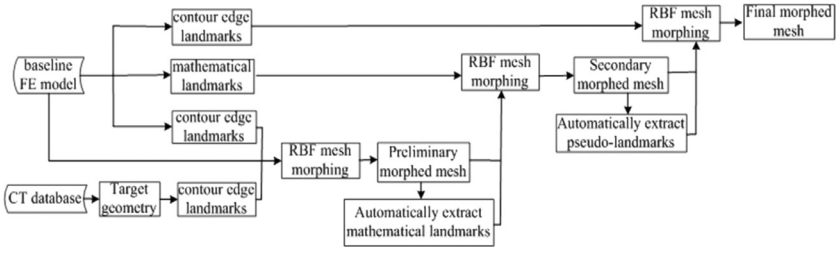

Figure 2. Procedure to develop the target FE mesh.

Table 2
Basic information of the target geometries and baseline models.

Target geometry	Geometry number	Age (year)	Mesh type	Mesh number	Node number	Mesh size (mm)
C5	No 1	9	Hexahedral element	1598	2422	1.6
	No 2	6				
R7	No 3	12		1853	2640	1.8
	No 4	4				
Femur	No 5	10		6420	10,224	3.0
	No 6	7				

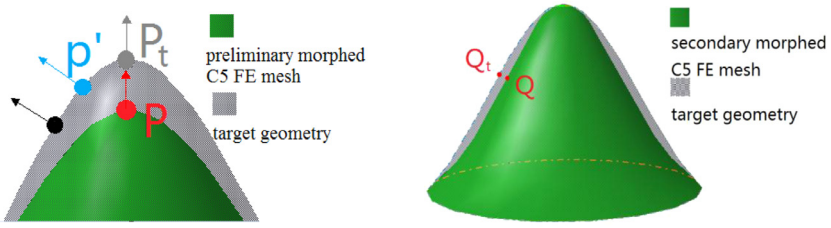

a) Extraction of mathematical landmarks b) Extraction of pseudo-landmarks

Figure 3. Automatic extraction landmarks.

distance from P was minimal, was calculated. Third, through a circumferential range of point P', points that were near P' were found and the unit normal vectors of these points were calculated. Last, the unit normal vector of P was compared to the unit normal vectors of these points. The angle of the point whose unit normal vector was closest to the unit normal vector of P was taken as Pt.

All 10 mathematical landmarks on the C5 target geometry corresponding to the C5 FE mesh were extracted automatically by this method. Using RBF mesh morphing based on 25 contour edge landmarks and 10 mathematical landmarks, the C5 FE mesh model was morphed into the C5 target geometry. Consequently, pseudo-landmarks on the C5 FE mesh were morphed into a position closer to the target geometry than the position obtained in preliminary morphing.

In the point cloud data, the unit normal vector algorithm of a point P is as follows:

(1) The points set around P

$$\begin{Bmatrix} x_1 & y_1 & z_1 \\ . & . & . \\ . & . & . \\ . & . & . \\ x_n & y_n & z_n \end{Bmatrix}$$

(2) The covariance of the points set:

$$\mathrm{cov}(x,\ y) = \frac{\sum_1^n (x_i - \bar{x})(y_i - \bar{y})}{n-1}$$

(3) Covariance matrix:

$$C = \begin{bmatrix} \mathrm{cov}\ (x,\ x) & \mathrm{cov}\ (x,\ y) & \mathrm{cov}\ (x,\ z) \\ \mathrm{cov}\ (y,\ x) & \mathrm{cov}\ (y,\ y) & \mathrm{cov}\ (y,\ z) \\ \mathrm{cov}\ (z,\ x) & \mathrm{cov}\ (z,\ y) & \mathrm{cov}\ (z,\ z) \end{bmatrix}$$

The eigenvalues and eigenvectors of the covariance matrix were calculated. The eigenvector corresponding to the minimum eigenvalue was the unit normal vector of point P.

2.4.4. Automatic extraction of pseudo-landmarks and final morphing

The method of automatically extracting pseudo-landmarks on the C5 target geometry corresponding to those on the C5 FE mesh is shown in Figure 3b. It is assumed that a pseudo-landmark Q was on the secondary morphed C5 FE mesh, and Qt on the C5 target geometry corresponded to Q. Point Qt whose distance from Q was minimal was taken as Qt. All 65 pseudo-landmarks on the C5 target geometry corresponding to the C5 baseline model were extracted automatically by this method.

After obtaining the pseudo-landmarks, volumetric mesh morphing was conducted according to 100 landmarks consisting of 25 contour edge landmarks, 10 mathematical landmarks and 65 pseudo-landmarks. Then a morphed model including 2D and 3D elements was obtained.

The numbers of contour edge landmarks, mathematical landmarks and pseudo-landmarks for the six target geometries are shown in Table 3. In the same kind of bone, the positions of landmarks correspond to each other. The baseline FE model was morphed into the target geometry based on the three kinds of landmarks.

The above processes were programmed in Scilab-5.5.2 (https://www.scilab.org).

2.5. The mesh quality, geometric accuracy and time consumption

To examine the mesh quality, three criteria (Jacobian $<$ 0.45, Warpage $>$ 60° and Skew $>$ 60°) were compared between the baseline model and the morphed FE mesh [21].

To quantify the geometric accuracy of the morphed FE model, all nodes on the surface of the morphed model were selected. The shortest distances between each node on morphed model and the target surface were calculated. The mean error, standard error (std. error), maximum error (max. error) and root mean square error (RSME) were used to evaluate the geometric accuracy [6,12].

Three operators, A, B and C, were selected to evaluate the geometric accuracy, the mesh quality of the morphed FE model and the time required to obtain all landmarks. The operator A was familiar with skeletal anatomy, and operators B and C had respectively intermediate and low levels of familiarity with skeletal anatomy, respectively, compared to A. Each of the operators extracted landmarks on six samples using the manual method and semi-automatic method. For each type of bone, the average time for extracting all landmarks from two samples was calculated.

2.6. The effect of proportional changes in the three types of landmarks

The effect of proportional changes in the three types of landmarks on the final morphed FE mesh was evaluated. Each type of landmark was increased or decreased by a scaling factor to

Table 3
The number of semi-automatically extracted landmarks.

Manual landmarks		C5		R7		Femur	
		No 1	No 2	No 3	No 4	No 5	No 6
		25	25	22	22	20	20
Automatic landmarks	Mathematical landmarks	10	10	16	16	16	16
	Pseudo-landmarks	65	65	40	40	106	106
SUM		100	100	78	78	142	142

Table 4
The effect of intra-operator variability on the geometric error through two methods (mm).

Geometry	Error	Method	Operator A	Operator B	Operator C	Average
C5	Mean	Full manual	0.564	0.585	0.605	0.585
		Semi-auto	0.521	0.557	0.529	0.536
	Max	Full manual	1.951	2.009	2.178	2.046
		Semi-auto	1.961	1.960	1.940	1.953
	SD	Full manual	0.321	0.328	0.334	0.328
		Semi-auto	0.310	0.344	0.320	0.324
	RMSE	Full manual	0.633	0.667	0.686	0.662
		Semi-auto	0.605	0.655	0.613	0.624
R7	Mean	Full manual	0.750	0.769	0.721	0.746
		Semi-auto	0.720	0.753	0.738	0.737
	Max	Full manual	2.789	3.377	3.277	3.148
		Semi-auto	2.685	2.939	2.789	2.804
	SD	Full manual	0.452	0.477	0.485	0.471
		Semi-auto	0.442	0.495	0.465	0.467
	RMSE	Full manual	0.928	0.956	0.913	0.932
		Semi-auto	0.844	0.882	0.849	0.858
Femur	Mean	Full manual	0.974	0.981	0.987	0.981
		Semi-auto	0.952	0.947	0.963	0.954
	Max	Full manual	3.326	3.418	3.372	3.372
		Semi-auto	3.078	3.086	3.094	3.085
	SD	Full manual	0.541	0.544	0.556	0.547
		Semi-auto	0.523	0.547	0.545	0.538
	RMSE	Full manual	1.118	1.144	1.157	1.139
		Semi-auto	1.055	1.067	1.081	1.068

Note: Three operators, A, B and C, were selected to evaluate the geometric accuracy using two methods. Operator A was familiar with skeletal anatomy, and operator B and operator C had intermediate and low levels of familiarity with skeletal anatomy, respectively, compared to operator A.

evaluate its effect on the geometric accuracy and mesh quality of the morphed FE mesh. “D” represents the proportion of one type of landmark decreased by a scaling factor of 0.8. “I” represents the proportion of one type of landmark increased by a scaling factor of 1.2. “U” represents the proportion of one type of landmark remaining unchanged, with a scaling factor of 1. Seven combinations of three types of landmarks, including UUU, DUU, UDU, UUD, IUU, UIU, and UUI, represented the scaling factors of contour edge landmarks, mathematical landmarks and pseudo-landmarks.

2.7. The effect of the mesh density

The effect of the mesh density of the baseline model on the geometric accuracy and mesh quality of the morphed model was evaluated. In order to maintain the original geometric accuracy and mesh quality of the baseline models, the elements were first split into 8 equal parts evenly. Then, a second split was conducted on the 8 parts again. Therefore, three mesh densities were used for evaluation.

3. Results

3.1. The geometric accuracy

The geometric accuracies of the models morphed by the full manual method and semi-automatic method with three operators are shown in Table 4. As each type of bone has two samples, the average geometry errors (mean, std. error, max. error and RMSE) of the two obtained morphed FE models were calculated and presented. In general, the geometric accuracies of the final morphed models obtained by the semi-automatic method and full manual method were similar. For the full manual method, the average mean error and max. error for the three operators were 0.77 and 2.06 mm, respectively. For the semi-automatic method, the average mean error and max. error for the three operators were 0.74 and 1.90 mm, respectively. The morphed FE model obtained by the semi-automatic method was compared with the target geometry, as shown in Figure 4.

3.2. Mesh quality

The mesh qualities of the morphed FE model obtained by the full manual method and semi-automatic method with three operators are shown in Appendix Table A1. It can be seen from the table that, after mesh morphing by the two methods, the percentages of failed elements for C5 (which has a complex geometry) were approximately 1–5%, which were higher than those of the baseline model (0%). The mesh qualities of the other samples (R7 and femur) were almost the same as those of the baseline model.

3.3. Comparison of the time consumption

The time for extraction of landmarks by using two methods and three operators with different levels of familiarity with skeletal

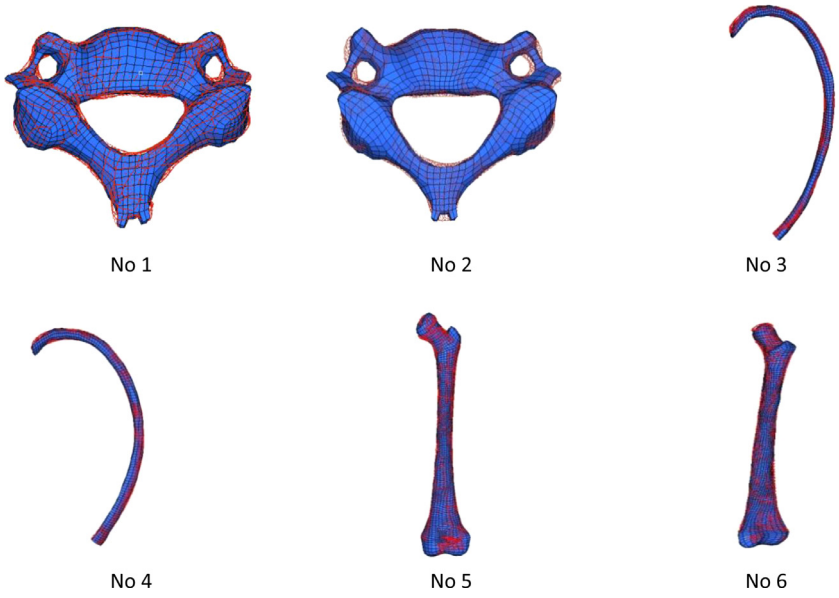

Figure 4. The morphing results.

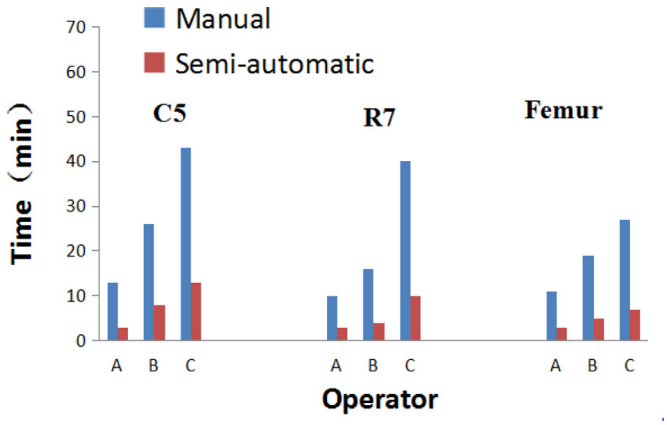

Figure 5. Comparison of the time consumption.

anatomy is shown in Figure 5. The operator familiar with skeletal anatomy can save at least 1/2 of the time of the operator with a low level of familiarity. The method of semi-automatically extracting landmarks saves 2/3 to 3/4 of the time relative to traditional manual extraction of landmarks for all three operators, regardless of familiarity with the skeletal anatomy.

3.4. The effect of proportional changes in the three types of landmarks

As shown in Appendix Table A2, for the three types of landmarks, reduction in the number of landmarks, as defined in Table 3, caused the geometric errors (mean error, std. error, max. error, and RSME) of the morphed model to increase by 1.4–37.2%, which indicated a decrease in geometric accuracy. With an increase in the number of contour edge landmarks, as defined in Table 3, the geometric errors increased by 0.8–28.7%, which also indicated a decreasing trend in geometric accuracy. With an increase in the number of mathematical landmarks or pseudo-landmarks, as defined in Table 3, the geometric errors decreased by −0.4% to 9.9%, which showed that the geometric accuracy of the morphed model was either unchanged or slightly increased.

As for the mesh quality of the morphed model, the effect of proportional changes in the three types of landmarks was not marked, as shown in Appendix Table A3.

3.5. The effect of mesh density

As for geometric accuracy, with an increasing mesh density in the baseline model, the mean error, std. error and RMSE error of the morphed model decreased by 0.77–28.5%, while the max. error increased by 4.8–13.6%. However, the mesh quality of the morphed model did not change markedly with changes in mesh density. The results are shown in Appendix Tables A4 and A5.

4. Discussion

Using the of RBF mesh morphing method to develop parametric human FE models was described in detail in previous studies [4,5,8]. However, it is very difficult and time-consuming to manually identify and extract thousands of corresponding landmarks on each target geometry. To reduce the time and improve the accuracy for identifying and extracting landmarks, Li et al. [22] developed a method that can automatically extract numerous landmarks from cranial CT scans. However, the method was applicable only for simple geometry, and was not suitable for complex geometry, such as the vertebrae and femur. For the method proposed in this study, the operator extracted only easy-to-identify contour edge landmarks, while mathematical landmarks and pseudo-landmarks were extracted automatically; therefore, this method it can be further applied to all human skeletons. The contour edge landmarks extracted on the target geometries are shown in Figure 6.

The purpose of classifying landmarks into three subgroups was to use different methods to rapidly and accurately identify these landmarks. The landmarks distributed on the bones are usually divided into anatomic and non-anatomic landmarks [5,8]. In this study, the anatomic landmarks were classified into contour edge landmarks and mathematical landmarks, and the non-anatomic landmarks were defined as the pseudo-landmarks. With the RBF method based on manually extracting contour edge landmarks, the

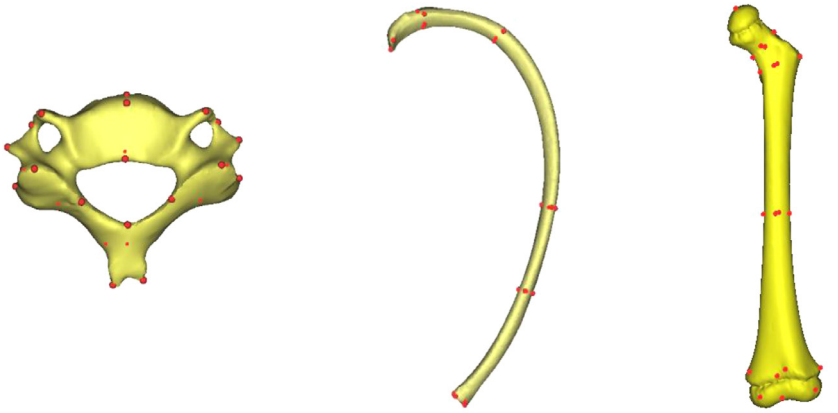

Figure 6. The contour edge landmarks on the target geometries.

coordinate of the morphed FE mesh and the point cloud data of the target geometry were approximately consistent. Then mathematical landmarks and pseudo-landmarks were extracted automatically with different algorithms.

Shi et al. [4] identified and extracted 40 landmarks manually on the seventh rib (R7) [4], and the mean geometry error was 0.98 mm. In this study, operators extracted only 22 contour edge landmarks on the seventh rib, and other landmarks were extracted automatically, which can significantly reduce the time for landmark extraction. In addition, the mean geometry errors of the two morphed R7 FE meshes (samples No. 3 and No. 4) was 0.61 and 0.52 mm, respectively, which indicated that the increase in the landmark extraction efficiency would not reduce the geometric accuracy of the morphed model. Bryan et al. [9] developed a statistical model of the femur by the surface matching method, and the mean geometry error was 0.598 mm. In this study, the average mean error of the two morphed femur FE models (samples No. 5 and No. 6) obtained from three operators was 0.87 mm, which showed a relatively lower geometric accuracy than the result from Bryan's study. However, it should be noted that the element used in Bryan's study was tetrahedral element, while the hexahedral element was used in this study. Tetrahedral elements are more suitable to fit complex geometry. The hexahedral element, however, allows more stable simulation results [23].

Currently, the landmark-based mesh morphing method is used to develop parametric human FE models that can enable safety design optimization for various vulnerable populations, such as children, small females, elderly occupants, and obese occupants [7,12,24,25]. Klein et al. [8] manually extracted 59 landmarks on each femur and a total of 5782 landmarks on 98 femur CT scans to develop a statistical femur geometry model. In this study, only 20 landmarks were manually extracted, and 112 landmarks were extracted automatically. Wang et al. [6] manually extracted 40 landmarks on each R7 target geometry and a total of 4040 landmarks on 101 R7 CT scans to develop a statistical rib geometry model. In this study, only 22 landmarks were extracted manually on R7 target geometry, and 56 landmarks were extracted automatically. Grassi et al. morphed the femur FE model to the specific geometry based on 10 landmarks. Due to the small number of landmarks, the preliminary morphed FE model has low geometric accuracy. To improve the geometric accuracy, the morphed model was projected to the targeted geometry through orthogonal projection. Obviously, the geometric accuracy of the final model was based on the result of preliminary mesh morphing. For human bone with complex geometry, such as cervical vertebrae, a small number of pre-selected landmarks cannot readily provide good agreement between morphed models and the target geometry. Therefore, the method presented by Grassi et al. [14] is more suitable for human bone with relatively simple geometry.

4.1. The effect of proportional change in the three types of landmark

With a few contour edge landmarks, when the number of contour edge landmarks increased, the preliminary morphing result improved. Then, the positions of mathematical and pseudo landmarks predicted by landmark extraction algorithms also improved. Consequently, the geometric accuracy of the final morphed model was improved. However, when the contour edge landmarks increased to a certain number, the position error of the landmark increased because more landmarks were extracted manually. Then, the geometric accuracy of the final morphed model decreased. In addition, the workload of selecting contour edge landmarks was also increased. Therefore, the number of contour edge landmarks should be determined according to the geometric accuracy of the morphed model and the workload of selecting landmarks.

With a few mathematical landmarks or pseudo-landmarks, increasing the number of any type of these landmarks improved the geometric accuracy of the final morphed model. When mathematical landmarks or pseudo-landmarks increased to a certain number, increasing the proportion of two types of landmarks, the geometric accuracy of the final morphed model was stable or slightly increased. In addition, increasing the number of mathematical or pseudo-landmarks, increased the time required to obtain all landmarks by the semi-automatic method. Therefore, a balance between geometric accuracy and computational time should be sought.

The proportional changes in the three types of landmarks have limited effects on mesh quality. In this study, the mesh quality is mainly determined by the position accuracy of the landmarks and the interpolating function used in the morphing method. Since the interpolating function was the same for all analyses, the mesh quality was mainly influenced by the position accuracy of the landmark. For the semi-automatic method, the contour edge landmarks were easily identified, and the mathematical landmarks or pseudo-landmarks were extracted by the algorithm. The position accuracy of the landmark can be ensured. Therefore, by using the semi-automatic landmark identification method, consistency of the mesh quality can be achieved. For the manual landmark

identification method, the use of different operators results in different position accuracies of the landmark, which influences the consistency of the mesh quality of the morphed model, as shown in Appendix Table A3.

4.2. The effect of mesh density

If the average element size is reduced, the morphed mesh can better fit the detailed features of the target geometry. Therefore, the mean error, std. error and RSME were reduced. The maximum error was calculated as the distance between a specific node on the morphed model and the target surface. With increasing mesh density, the node approached closer to the position with the maximum distance between the morphed model and target geometry. Therefore, the maximum error increased with increasing mesh density. Furthermore, with increasing mesh density, the time required to obtain all landmarks by the semi-automatic method increased.

As mentioned above, in this study, the mesh quality was mainly determined by the position accuracy of the landmarks. In the study of exploring the effect of mesh density on mesh quality, the positions of the landmarks were not changed; thus, the mesh quality was not changed.

This study has several limitations. First, the accuracy of automatically extracting landmarks is related to the interval between CT slices. The 3D target geometry was obtained through the CT data, and the landmarks were extracted on the reconstructed target geometry. For bone with very small geometry features, such as the cervical bone of an infant, some geometry features could be lost due to the interval between CT slices. Second, before calculating the unit normal vector of a point, point set near the point need to be assigned. However, the size of a suitable point set is uncertain. It is necessary to adjust this size according to the interval between CT slices and the complexity of the target geometry. In this study, the size of the point set was set to 3 mm in diameter empirically. Third, although many landmarks are automatically extracted, it is necessary to extract contour edge landmarks manually. If the sample size is very large, selecting contour edge landmarks is still a heavy workload. Therefore, future improvement can be made in using fewer manually extracted landmarks or developing a fully automatically extracting method.

5. Conclusion

In this study, a new method was developed to semi-automatically extract landmarks. The method required manual extraction only of easy-to-identify contour edge landmarks. Mathematical landmarks and pseudo-landmarks were automatically extracted by the custom algorithm. The application of the method can effectively reduce the time for identifying landmarks without sacrificing geometric accuracy and mesh quality in the process of developing parametric FE models with complex geometry.

Conflict of interest

None declared.

Ethics approval

Ethical approval was obtained by an institutional review board: the Third Xiangya Hospital of Central South University (Approval number: 2017-S270).

Acknowledgments

This work was supported by the National Natural Science Foundation of China (Award no. 51505137), the State Key Laboratory of Advanced Design and Manufacturing for Vehicle Body at Hunan University (Award no. 31615007), and the Training Program for Excellent Young Innovators of Changsha (Award no. kq1802009). The authors would like to thank Dr. Yin Liu for their support on the CT image 3D reconstruction.

Appendix

Table A1
The effect of intra-operator variability on mesh quality through two methods (percentage, and number of failure elements).

Geo-metry	Mesh quality	Method	Baseline	Operator A	Operator B	Operator C	Average
C5	Jacobian < 0.45	Full manual	0%(2)	2%(28)	3%(43)	3%(46)	2.7%(39)
		Semi-auto	0%(2)	1%(16)	1%(12)	1%(28)	1.0%(18)
	Warpage > 60°	Full manual	0%(0)	2%(33)	3%(49)	3%(50)	2.7%(44)
		Semi-auto	0%(0)	1%(21)	1%(21)	1%(11)	1.0%(18)
	Skew > 60°	Full manual	0%(0)	1%(20)	4%(62)	4%(65)	3.0%(49)
		Semi-auto	0%(0)	3%(49)	3%(42)	2%(27)	2.4%(39)
R7	Jacobian < 0.45	Full manual	1%(11)	1%(12)	0%(16)	1%(18)	0.7%(15)
		Semi-auto	1%(11)	1%(12)	1%(14)	1%(15)	1%(13)
	Warpage > 60°	Full manual	0%(0)	0%(0)	0%(0)	0%(0)	0.0%(0)
		Semi-auto	0%(0)	0%(0)	0%(1)	0%(0)	0.0%(0)
	Skew > 60°	Full manual	0%(0)	0%(2)	0%(3)	0%(2)	0.0%(2)
		Semi-auto	0%(0)	1%(10)	0%(3)	0%(6)	0.3%(6)
Femur	Jacobian < 0.45	Full manual	0%(29)	0%(32)	0%(27)	0%(30)	0.0%(30)
		Semi-auto	0%(29)	0%(27)	0%(27)	0%(30)	0.0%(28)
	Warpage > 60°	Full manual	0%(0)	0%(0)	0%(3)	0%(8)	0.0%(3)
		Semi-auto	0%(0)	0%(0)	0%(0)	0%(9)	0.0%(3)
	Skew > 60°	Full manual	0%(0)	0%(2)	0%(7)	0%(11)	0.0%(7)
		Semi-auto	0%(0)	0%(2)	0%(2)	0%(7)	0.0%(3)

Table A2
The effect of proportional change in the 3 types of landmarks on the geometric error (mm).

Geometry	Error	UUD	UDU	DUU	UUU	IUU	UIU	UUI
C5	Mean	0.545	0.552	0.594	**0.521**	0.533	0.520	0.504
	Max	2.035	2.060	2.373	**1.961**	2.524	1.969	1.935
	SD	0.315	0.324	0.371	**0.310**	0.328	0.312	0.298
	RMSE	0.625	0.640	0.700	**0.605**	0.626	0.602	0.585
R7	Mean	0.757	0.750	0.776	**0.720**	0.731	0.715	0.717
	Max	3.636	2.989	3.683	**2.685**	2.719	2.655	2.660
	SD	0.483	0.475	0.541	**0.442**	0.463	0.440	0.438
	RMSE	0.898	0.857	0.946	**0.844**	0.856	0.840	0.842
Femur	Mean	0.972	0.969	0.965	**0.952**	0.968	0.907	0.914
	Max	3.160	3.125	3.411	**3.078**	3.102	2.895	2.905
	SD	0.539	0.573	0.538	**0.523**	0.537	0.471	0.522
	RMSE	1.135	1.178	1.187	**1.055**	1.162	0.946	1.049

Note: Seven combinations of three types of landmarks, including UUU, DUU, UDU, UUD, IUU, UIU, and UUI, represent the scaling factor of the number of contour edge landmarks, mathematical landmarks and pseudo-landmarks. "D" represents the proportion of landmarks decreasing by a scaling factor of 0.8. "I" represents the proportion of landmarks increasing by a scaling factor of 1.2. "U" represents the proportion of landmarks remaining unchanged, with the scaling factor equal to 1. For example, UUD represents scaling factors of the number of contour edge landmarks, mathematical landmarks and pseudo-landmarks of 1.0, 1.0 and 0.8, respectively.

Table A3
The effect of proportional change in the 3 types of landmarks on the mesh quality (mm).

Geo-metry	Mesh quality	Baseline	UUD	UDU	DUU	UUU	IUU	UIU	UUI
C5	Jacobian < 0.45	0%(2)	2%(25)	1%(22)	0%(6)	**1%(16)**	1%(15)	2%(35)	2%(33)
	Warpage > 60°	0%(0)	1%(21)	1%(18)	1%(16)	**1%(21)**	1%(16)	1%(21)	1%(22)
	Skew > 60°	0%(0)	6%(93)	6%(90)	7%(117)	**3%(49)**	2%(34)	3%(48)	3%(62)
R7	Jacobian < 0.45	1%(11)	1%(15)	1%(17)	1%(15)	**1%(16)**	1%(13)	1%(16)	1%(16)
	Warpage > 60°	0%(0)	0%(0)	0%(0)	0%(0)	**0%(0)**	0%(0)	0%(0)	0%(0)
	Skew > 60°	0%(0)	1%(10)	1%(12)	0%(2)	**1%(10)**	0%(2)	1%(12)	1%(10)
Femur	Jacobian < 0.45	0%(29)	0%(28)	0%(27)	0%(29)	**0%(27)**	0%(26)	0%(26)	0%(30)
	Warpage > 60°	0%(0)	0%(0)	0%(0)	0%(0)	**0%(0)**	0%(0)	0%(0)	0%(0)
	Skew > 60°	0%(0)	0%(2)	0%(2)	0%(2)	**0%(2)**	0%(3)	0%(8)	0%(0)

Table A4
The effect of the mesh density on the geometric error (mm).

Geometry	Error	Low density (Original Model)	Medium density (1st split)	High density (2nd split)
C5	Mean	0.521	0.515	0.517
	Max	1.961	2.072	2.130
	SD	0.310	0.269	0.268
	RMSE	0.605	0.581	0.582
R7	Mean	0.720	0.611	0.612
	Max	2.685	3.012	3.050
	SD	0.442	0.322	0.316
	RMSE	0.844	0.690	0.689
Femur	Mean	0.952	0.943	0.941
	Max	3.078	3.225	3.274
	SD	0.523	0.460	0.453
	RMSE	1.055	0.987	0.984

Note: Three mesh densities of baseline models were used for evaluating the geometric accuracy. In order to keep the original geometric accuracy and mesh quality of the baseline models, the elements were first split into 8 equal parts evenly for a medium density of the morphed model. Then, a second split was applied to the 8 parts again for a high density of the morphed model.

Table A5
The effect of mesh density on mesh quality (percentage, and numbers of failure elements).

Geo-metry	Mesh quality	Low density (Original Model)		Medium density (1st split)		High density (2nd split)	
		Baseline1	Target	Baseline2	Target	Baseline3	Target
C5	Jacobian < 0.45	0%(2)	1%(16)	0%(2)	0%(3)	0%(0)	0%(0)
	Warpage > 60°	0%(0)	1%(21)	0%(0)	0%(7)	0%(0)	0%(0)
	Skew > 60°	0%(0)	3%(49)	0%(0)	2%(297)	0%(28)	4%(4355)
R7	Jacobian < 0.45	1%(11)	1%(16)	0%(0)	0%(0)	0%(0)	0%(0)
	Warpage > 60°	0%(0)	0%(0)	0%(0)	0%(0)	0%(0)	0%(0)
	Skew > 60°	0%(0)	1%(10)	0%(0)	0%(10)	0%(80)	0%(0)
Femur	Jacobian < 0.45	0%(29)	0%(27)	0%(2)	0%(2)	0%(0)	0%(0)
	Warpage > 60°	0%(0)	0%(0)	0%(0)	0%(0)	0%(0)	0%(0)
	Skew > 60°	0%(2)	0%(0)	0%(0)	0%(29)	0%(4)	0%(147)

Note: Baseline 1 was the original baseline model. Baseline 2 was obtained through splitting baseline model 1. Baseline 3 was obtained through splitting baseline model 2. For C5, the element numbers of baseline1, baseline2, and baseline3 were 1598, 12,784 and 102,272, respectively. For R7, the element numbers of baseline1, baseline2, and baseline3 were 1853, 14,824, 118,592, respectively. For the femur, the element numbers of baseline1, baseline2, and baseline3 were 6420, 51,360 and 410,880, respectively.

References

[1] Carr JC, Fright WR, Beatson RK. Surface interpolation with radial basis functions for medical imaging. IEEE Trans Med Imaging 1997;16(1):96–107.
[2] Besnault B, Lavaste F, Guillemot H, et al. A parametric finite element model of the human pelvis; 1998. SAE Technical Paper p. 0148–7191.
[3] Li Z, Hu J, Reed MP, et al. Development, validation, and application of a parametric pediatric head finite element model for impact simulations. Ann Biomed Eng 2011;39(12):2984–97.
[4] Shi X, Cao L, Reed MP, et al. A statistical human rib cage geometry model accounting for variations by age, sex, stature and body mass index. J Biomech 2014;47(10):2277–85.
[5] Li Z, Park B-K, Liu W, et al. A statistical skull geometry model for children 0-3 years old. PLoS One 2015;10(5):e0127322.
[6] Wang Y, Cao L, Bai Z, et al. A parametric ribcage geometry model accounting for variations among the adult population. J Biomech 2016;49(13):2791–8.
[7] Zhang K, Cao LB, Fanta A, et al. An automated method to morph finite element whole-body human models with a wide range of stature and body shape for both men and women. J Biomech 2017;60:253–60.
[8] Klein KF, Hu J, Reed MP, et al. Development and validation of statistical models of femur geometry for use with parametric finite element models. Ann Biomed Eng 2015;43(10):2503–14.
[9] Bryan R, Mohan PS, Hopkins A, et al. Statistical modelling of the whole human femur incorporating geometric and material properties. Med Eng Phys 2010;32(1):57–65.
[10] Bucki M, Lobos C, Payan Y. A fast and robust patient specific Finite Element mesh registration technique: application to 60 clinical cases. Med Image Anal 2010;14(3):303–17.
[11] Couteau B, Payan Y, Lavallee S. The mesh-matching algorithm: an automatic 3D mesh generator for finite element structures. J Biomech 2000;33(8):1005–9.
[12] Hu J., Klein K., Li Z., et al. Developing parametric human models representing various vulnerable populations in motor vehicle crashes. The 18th China Conference of Automotive Safety Technology; 2015.
[13] Hu J, Rupp JD, Reed MP. Focusing on vulnerable populations in crashes: recent advances in finite element human models for injury biomechanics research. J Automot Saf Energy 2012;3:295–307.
[14] Grassi L, Hraiech N, Schileo E, et al. Evaluation of the generality and accuracy of a new mesh morphing procedure for the human femur. Med Eng Phys 2011;33(1):112–20.
[15] Dong L, Li G, Mao H, et al. Development and validation of a 10-year-old child ligamentous cervical spine finite element model. Ann Biomed Eng 2013;41(12):2538–52.
[16] Dong L, Mao H, Li G, et al. Investigation of pediatric neck response and muscle activation in low-speed frontal impacts. Comput Methods Biomech Biomed Eng 2015;18(15):1680–92.
[17] Jiang B, Cao L, Mao H, et al. Development of a 10-year-old paediatric thorax finite element model validated against cardiopulmonary resuscitation data. Comput Methods Biomech Biomed Eng 2014;17(11):1185–97.
[18] Jiang B, Mao H, Cao L, et al. Experimental validation of pediatric thorax finite element model under dynamic loading condition and analysis of injury; 2013. SAE Technical Paper p. 0148–7191.
[19] Shen M, Zhu F, Mao H, et al. Finite element modelling of 10-year-old child pelvis and lower extremities with growth plates for pedestrian protection. Int J Vehicle Safety 2015;8(3):263–86.
[20] Shen M, Zhu F, Jiang B, et al., editors. Development and a limited of whole–body finite element pedestrian and occupant models of a 10-year-old child, Proceedings of the international research council on biomechanics of injury conference (IRCOBI); 2015.
[21] Li Z, Hu J, Zhang J, editors. Comparison of different radial basis functions in developing subject-specific infant head finite element models for injury biomechanics study, Proceedings of the ASME 2012 summer bioengineering conference. American Society of Mechanical Engineers; 2012.
[22] Li Z, Han X, Ge H, et al. A semi-automatic method of generating subject-specific pediatric head finite element models for impact dynamic responses to head injury. J Mech Behav Biomed Mater 2016;60:557–67.
[23] Ramos A, Simões JA. Tetrahedral versus hexahedral finite elements in numerical modelling of the proximal femur. Med Eng Phys 2006;28(9):916–24.
[24] Hwang E, Hallman J, Klein K, et al. Rapid development of diverse human body models for crash simulations through mesh morphing; 2016. SAE Technical Paper p. 0148–7191.
[25] Zhang K, Cao LB, Wang YL, et al. Impact response comparison between parametric human models and postmortem human subjects with a wide range of obesity levels. Obesity 2017;25(10):1786–94.